ChemPhysChem

Research Article
doi.org/10.1002/cphc.202300180

Chemistry Europe
European Chemical Societies Publishing

www.chemphyschem.org

Eutectic Media Open a Synthetic Route to Oligocitrazinic Acid Fluorophores of Purple Hue

Helen Schneider,[a] Volker Strauss,[a] Sarah Vogl,[b] Markus Antonietti,[a] and Svitlana Filonenko*[a]

Under isochoric and solvent-free conditions, the reaction between ammonium formate and citric acid results in a deeply purple reaction product with fluorescent properties. This brings this reaction in the realm of bio-based fluorophores and bottom-up carbon nanodots from citric acid. The reaction conditions are optimized in terms of UV–vis spectroscopic properties and, subsequently, the main reaction product is separated. While the structural analysis does not give any indication for carbon nanodots in a general sense, it points towards the formation of molecular fluorophores that consist of oligomerized citrazinic acid derivatives. Furthermore, EPR spectroscopy reveals the presence of stable free radicals in the product. We hypothesize that such open-shell structures may play a general role in molecular fluorophores from citric acid and are not yet sufficiently explored. Therefore, we believe that analysis of these newly discovered fluorophores may contribute to a better understanding of the properties of fluorophores and CND from citric acid in general.

Introduction

Research on fluorophores from citric acid (CA) and reactive nitrogen precursors has been a flourishing subject in recent years. Such materials are promising due to their sustainable, bio-based precursors and their intriguing fluorescent properties, which make them attractive for many applications such as in biomedical imaging,[1–4] fluorescent inks,[5,6] solar cells[7–9] or fluorescent probes for detection of metals and biomolecules.[10–14]

The starting point for the research on CA derived fluorophores was already marked in the late 19th century by the discovery of the molecular fluorophore citrazinic acid (CzA). Behrmann and Hoffmann synthesized it in 1884 by the addition of sulphuric acid to a water solution of citric acid amide.[15] Two years later, Sell and Easterfield obtained CzA by the reaction of CA with ammonia via melt formation by evaporation of water.[16,17] Heating the resulting melt to 130 °C led to transformation of ammonium citrate into its amide and substantially to CzA. This method was widely used to synthetize CzA, particularly for colour photography films processing such as Kodak Ektachrome E-6 process.[18] After the synthesis of Sell and Easterfield, it has been observed that CA can form many fluorescent structures, using different amines instead of ammonia as reactants. Many of such CzA derivatives have been reported by Kaspzyk et al.[19]

In recent years, considerable research on fluorescent materials form CA has been performed under the headline of carbon nanodots (CNDs).[20] Currently, the structure of CNDs is typically depicted as a core/shell model, where a carbon core with graphitic elements is equipped with various functional groups on its surface.[21–23] CNDs from CA and various amines are typically formed by heating to temperatures between 140 and 200 °C, where solvent-free as well as hydro- and solvothermal approaches have been reported.[24,25]

The fluorescent properties of bottom-up CNDs from CA are still a matter of debate. They have been attributed to the graphitic core as well as to molecular fluorophores – namely CzA and its derivatives. However, it is still an open question how these fluorophores are connected to the cores of CNDs or with each other, or whether they are chemically connected at all.[20,26,27] Firstly, separation is an issue and in several cases the observed fluorescence could be attributed to a specific molecular species rather than CNDs after careful separation of the product mixture.[28,29] Secondly, aggregation plays an important part in the fluorescent properties of such molecules. For example, in 2017 Reckmeier et al.[30] analysed amorphous aggregates of CzA derivatives and showed that such aggregates could absorb and emit at wavelengths over a wide range of the visible spectra. The emission spectra was overall very similar to those typically reported for CNDs. In summary, one can say that fluorophores and CNDs from CA still pose a puzzle with respect to their structural analysis.

In this paper, we report on a novel synthesis, using CA and ammonium formate (AF) as reactants in an autoclaved solvent-free synthesis. This synthesis is especially interesting as it produces a dye substance with an intense purple colour, indicating a yet undiscovered reaction pathway. In most of the reported syntheses with CA so far, the reaction mixture has usually a brownish colour and is pale-yellow after dilution and

[a] H. Schneider, Dr. V. Strauss, Prof. Dr. Dr. h.c. M. Antonietti, Dr. S. Filonenko
Max Planck Institut für Kolloid- und Grenzflächenforschung Am Mühlenberg 1, 14476 Potsdam, Germany
E-mail: svitlana.filonenko@mpikg.mpg.de
[b] Dr. S. Vogl
Department of Chemistry/Functional Materials, Technische Universität Berlin, Hardenbergstraße 40, 10623 Berlin, Germany

Supporting information for this article is available on the WWW under https://doi.org/10.1002/cphc.202300180

purification.[31] However, red coloured CNDs also have been previously reported.[32,33] We hypothesize that formic acid plays a pivotal catalytic role in the system, which results in subsequent oligomerization of CzA derivatives.

Results and Discussion

Synthesis in Eutectic Mixture

We recently discovered that AF is able to form eutectic mixtures with many hydrogen bond donors.[34,35] Those mixtures have commonalities with eutectic mixtures of Lewis acids and bases commonly referred as deep eutectic solvents (DES) due to their similarities with ionic liquids. Namely, eutectic mixtures containing AF are liquid at relatively low temperatures and show typical glass transition of a one-phase system. The peculiarity of those eutectics is the reactivity of AF, which enables solvent-free reactions and which brings those systems in the category of reactive eutectic mixtures. AF and CA (2:1) form a eutectic mixture that is liquid at room temperature (with a glass transition temperature at −37.1 °C) and that starts reacting at elevated temperatures (Figure S1). The unique properties of the system are related to the preservation of the phase unity in the homogeneous liquid state moving over the reaction coordinate, despite composition change due to the evolution of reaction products. The incorporation of the low molecular weight compounds into eutectic is supported by the DCS analysis that reveals a single glass transition at temperatures decreasing upon applying higher reaction temperatures (Figure S1). Considering that formic acid (FA) and CA are acids both of similar strength we can assume that the ammonium cation is shared between both acids but the exchange equilibrium is shifted towards ammonium citrate if the temperature is high enough to bring FA into the vapour phase. The ammonium salt of CA can then form CzA at a suitable temperature. Indeed, at 120 °C we can observe a colour change of the reaction mixture into yellow, which is in agreement with the reported preparation of CzA from CA and ammonia or urea at 120–130 °C.[36] Thermal analysis together with FTIR and NMR of the reaction mixtures prepared at temperatures above 120 °C reveals the similarities in the composition of the mixtures and the unity in the behaviour implying incorporation of the possible products into the eutectic (Figures S3–S6). At 150 °C, the mixture starts to get a purple hue while at 180 °C an intense purple colour is observed (Figure 1, left). This is a common synthesis temperature for fluorophores from CA since it starts to decompose above 175 °C and reaction kinetics are accelerated.[29] Furthermore, in our system AF decomposes at 180 °C, so at this temperature a maximum concentration of ammonia can be expected. For the reaction, it is important to maintain isochoric conditions – the reaction does not work in an open vessel. Furthermore, the solvent-free approach appears to be essential for the synthesis – the same reaction in water results in a completely different reaction pathway, while the same reaction in ethylene glycol gives only traces of the relevant product, according to UV–vis (Figure S2). Solvent-free reactions are known to offer remarkable advantage, when compared to solution reactions because of the change in reaction kinetics. This is because collisions between the reactants are much more frequent and give higher reaction rates, which often results in high purity of the products with high selectivity.[35,37–39]

Reaction kinetics, monitored over time by UV–vis absorption spectroscopy (Figure 1, right), show a similar trend. The band at 340 nm (associated with CzA) develops initially but decreases over time in favour of an increasing band intensities at 520 and 560 nm. This reflects the purple colour of the resulting compound, reaching its maximum after a reaction time of four hours. Prolonged heating reduces the brilliance of colour.

Overall, the kinetic study shows that the reaction proceeds in at least two clearly distinguishable steps. The first one can be attributed to the formation of CzA (and derivatives) and the second one corresponds to the polymerization of the formed monomer into oligomers of purple hue. Based on these observations, we propose the following reaction products, depicted in Figure 2a, as a starting point for discussion. That products from CA are able to form such conjugated structures has long been known by the biosynthesis of indigoidine from CA.[40,41] Furthermore, indigoidine derivatives have recently been identified as reaction products from CA and urea by including a photo oxidation step during the synthesis.[42]

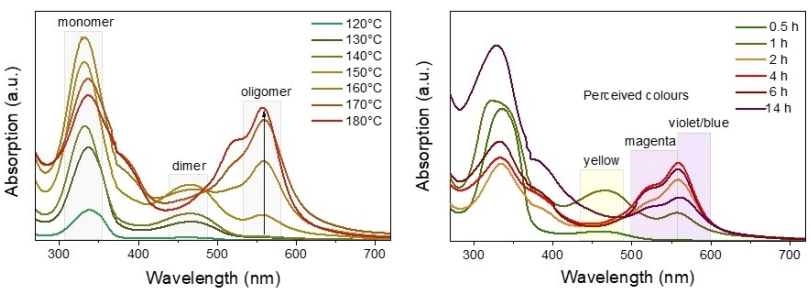

Figure 1. UV–vis spectra of the reaction kinetics of the reactive eutectics in water. Left: prepared at different temperatures from 120 to 180 °C and reacted for 40 min in a microwave oven. Right: prepared with different reaction times at a temperature of 180 °C in an autoclaved system. The maxima at ~340 nm corresponds to CzA.

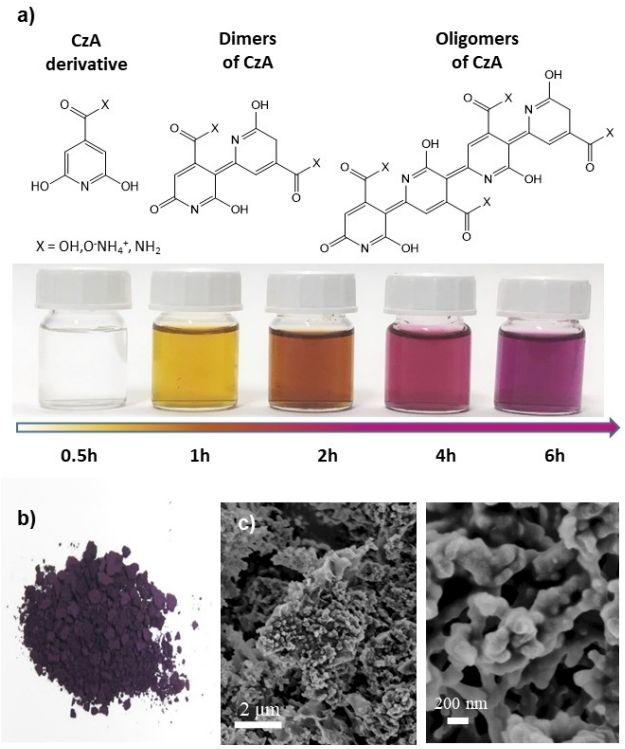

Figure 2. (a) Schematic representation of the formation kinetics of CzA and polymerization in the reactive eutectic media at 180 °C supported by the colour change of the reaction mixture, (b) visual appearance of the purified product **oligo-CzA** in powder form, (c) SEM images of the purified product.

Structural Analysis of the Fluorophores

In the following, the purple reaction product is investigated which is termed **oligo-CzA** in the further discussion. Maximum yields are obtained in an autoclaved synthesis at 180 °C for 4 h as shown by UV–vis analysis (or in 40 minutes in the microwave, which enables stirring). The reaction work-up can be easily achieved by repeated washing with ethanol. This precipitates the product and removes by-products such as formamide and formic acid as confirmed by nuclear magnetic resonance spectroscopy (NMR) (Figure S7). After drying, a purple powder of **oligo-CzA** is obtained (Figure 2B).

In the further analysis of the product, we did not find any indication of CNDs. Gel-permeation chromatography (GPC) shows only small sized molecules below the smallest standard of 1250 Da. Moreover, scanning electron microscopy (SEM) and transition electron microscopy (TEM) measurements (Figure 2C and Figure S9) do not reveal any crystalline particles, instead show amorphous agglomerates. This is in agreement with the finding of Reckmeier et al.,[31] who obtained similar TEM images for the reaction of CA and supercritical ammonia. They also attributed the observed particles to aggregated CzA derived fluorophores instead of CNDs.

NMR analysis of the product is not possible as the sample turns out to be completely NMR silent (Figure S7). EPR measurements (Figure 3, left) reveal that this is due to the paramagnetic nature of the product. The number of unpaired electrons in **oligo-CzA** is calculated to be $1.6\times10^{[18]}$ spins/g and increases slowly over time (Table S1). EPR measurements for variable temperatures reveal that the signal increases linearly with temperature, which means that the behaviour is Curie like (Figure 3, right). It is not the first time that EPR active CNDs or fluorophores from citric acid have been reported.[43,44] Interestingly, the ammonium salt of CzA (**NH_4-CzA**) also gives a weak EPR signal (Figure 3, left). The concentration of unpaired electrons is significantly lower at $5.1\times10^{[16]}$ spins/g. Both samples have very similar g-factors: 2.0036 for **oligo-CzA** and 2.0038 for **NH_4-CzA** (Figure S10). This indicates a similar chemical environment of the free radical in the two samples. Considering this result from a broader perspective, it may have important implications. If such open-shell structures also form in other syntheses with CA in the realm of CNDs, a portion of molecules may have been systematically overlooked in NMR analysis.

Regarding the cause of the observed radical stability we can only speculate here, but it must ultimately be traced back to the delocalization of spin density in the molecular structure.[45] This is known e.g. to be possible by extension of π-conjugates[46] (which is in fact featured by the proposed structure of **oligo-CzA**) but also possible by non-covalent mechanisms such as electrostatic interactions[47] or π–π interaction and molecular aggregates.[48] Also such non-covalent mechanisms seem worth to consider, taking into account that

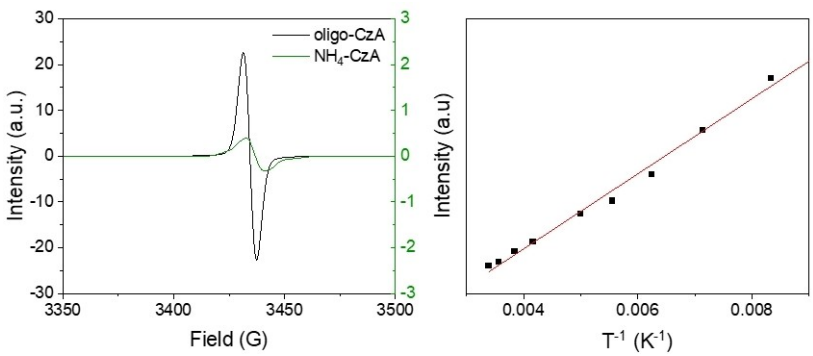

Figure 3. (left) EPR measurement of 20 mg of **oligo-CzA** and **NH_4-CzA**, (right) variable temperature EPR of **oligo-CzA**.

molecular aggregation of CzA has been identified as a crucial factor for understanding its fluorescent properties.[30]

For a better understanding of the observed radical stability, more analysis will be needed. E.g. it would be very interesting to perform magnetic susceptibility measurements in order to determine the ground state spin multiplicities of the system. We also tried to reduce **oligo-CzA** with sodium sulphite or to oxidize it with sodium hypochlorite – however the NMR remained silent in both cases. While reduction does not do anything to the colour, oxidation leads to a change in colour from purple to orange to yellow to colourless. This exactly the reversal of the formation kinetics, observed during synthesis.

The product is structurally investigated by X-ray photoelectron spectroscopy (XPS) in reference to **NH_4-CzA**, since similarities between the structures are presumed. The tautomeric forms of both structures are presented in Figure S11 to make it easier to follow the discussion. XPS results are shown in Figure 4.

The XPS C_{1s} spectra show four species of carbons within the compounds. For **oligo-CzA** they appear at 284.8, ~286, ~287.5 and ~288.5 eV and are assigned to carbon-carbon (C–C/C=C), hydroxy and carbon-nitrogen (C–O/C–N), carbonyl as well as lactam (C=O) and carboxy groups (O–C=O), respectively. For **NH_4-CzA** a significantly higher signal at 287.8 eV is observed in comparison to the oligomer suggesting that the lactam form is favoured over the pyridinic tautomer. This assumption is supported by the N_{1s} XPS spectrum presenting an intense signal at 400.6 eV which is characteristic for pyrrolic nitrogens and which is also in accordance with previous observations.[49] The N_{1s} spectrum of **oligo-CzA** shows a signal at 399.9 eV which indicates a mixture of pyridinic N which range between 399.0–399.6 eV as well as pyrrolic N at ~400.2 eV. This means that both tautomeric forms are present. Furthermore, the signals between 401.9–402.0 eV in both N_{1s} spectra prove the presence of ammonium ions. Due to the measurement under high vacuum, the amount of ammonia groups was possibly reduced to some extent for both compounds. Nevertheless, the small signal for **oligo-CzA** may also hint to the formation of primary amides from ammonium carboxylates which can be expected under such the high synthesis temperatures. Primary amides occur at ~399.7 eV and are therefore be part of the major signal at 399.9 eV. The O_{1s} spectra show two species at 531.7 and 533.2–533.4 eV which correspond with carbonyl as well as lactam groups (C=O/NH–C=O) and carboxyl as well as hydroxyl groups (O–C=O/C–OH), respectively. For **oligo-CzA** the reduction in intensity of the carboxyl/hydroxyl group signals at 533.2 eV is in accordance with the proposed structure and a decrease in hydroxyl groups as well as amide formation.

Similarities between **NH_4-CzA** and **oligo-CzA** are also observed with Fourier-transform infrared spectroscopy (FTIR), as shown in Figure 5 (similarly, eutectics prepared at different temperature and reaction mixture at different reaction time on Figures S6 and S8). What can clearly be distinguished in the **oligo-CzA** spectra are different C=O stretching vibrations. The peak at 1570 cm^{-1} corresponds with the peak of **NH_4-CzA** and is therefore assigned to the stretching of C=C bond conjugated with carboxylate group. The signal at 1690 cm^{-1} is assigned to the C=O stretching from carboxylic acid. Presumably, there were not sufficient ammonium ions present in order to ionise all carboxylic acid groups. This is supported by performing the synthesis of **oligo-CzA** with an excess of AF. In this case the signal at 1690 cm^{-1} from carboxylic acid disappears in favour of

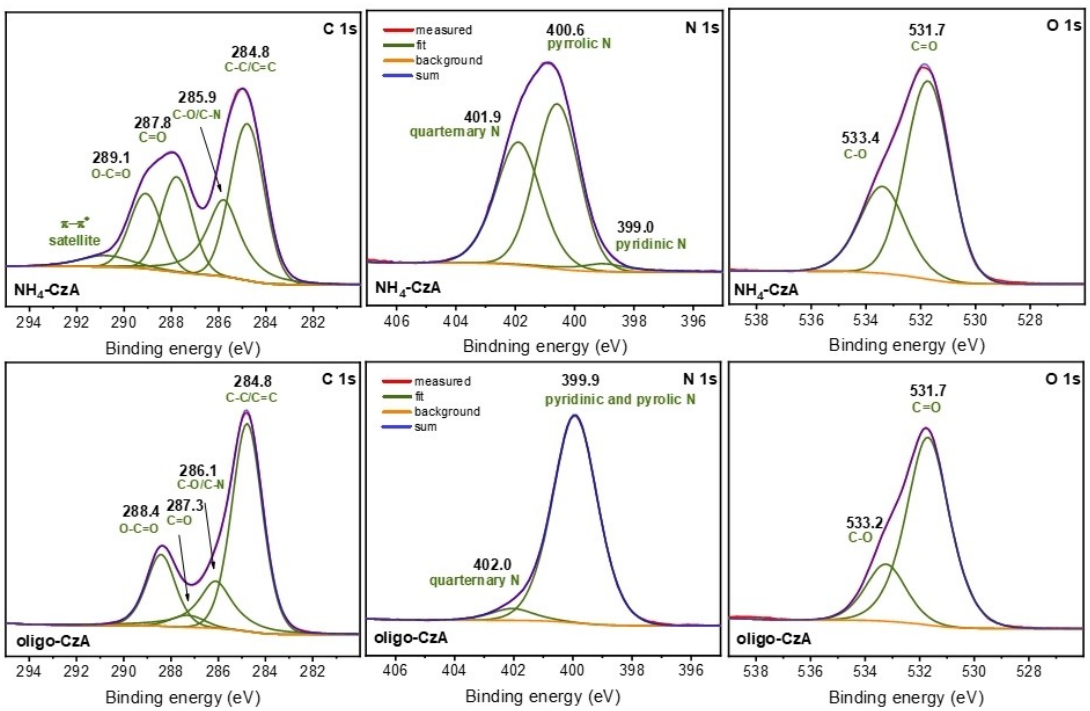

Figure 4. XPS spectra of **NH_4-CzA** (top) and purified **oligo-CzA** (bottom) with emphasis on the C_{1s}, N_{1s}, and O_{1s} regions.

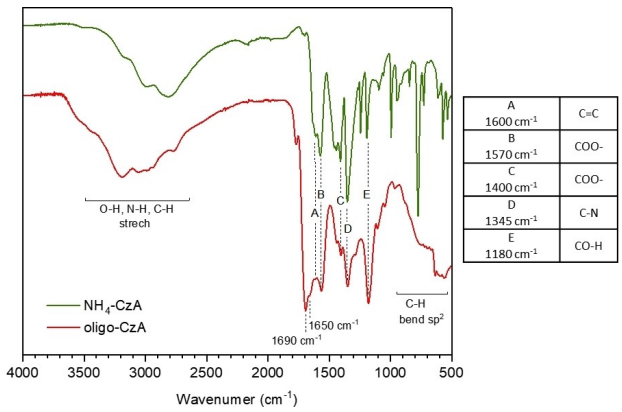

Figure 5. ATR-FTIR of **NH_4-CzA** and **oligo-CzA.**

a stronger signal from carboxylate stretching vibrations (Figure S7).

The same can be achieved, when **oligo-CzA** is treated with an alkali salt such as potassium or sodium hydroxide (Figure S12). This does not only result in salt formation of carboxylic acids but also in the cation exchange of ammonium ions as wells as hydrolysis of primary amides. In this way all derivatives of carboxylic acid groups are converted to the carboxylate salt of the respective alkali metal and the elemental analysis of these materials gives insightful results. While untreated **oligo-CzA** gives a nitrogen/carbon ratio of 1.6/6, the ratio of the alkali treated compound approaches 1:6, while the ratio between nitrogen and counter cation approaches 1:1. (Table S2) That means that each pyridine unit is connected to one carboxylate group, which reflects the structure of **NH_4-CzA**. This is in agreement with the proposed structure for **oligo-CzA** of polymerized CzA derivatives into oligomers.

For information on the molecular mass, MALDI-TOF (matrix-assisted laser desorption-ionization – time of flight) mass spectrometry experiments were performed. Although mostly used for large molecules such as synthetic polymers and proteins, this technique is also suitable for small molecular analytes. Soltzberg et al. successfully used MALDI-TOF mass spectrometry for the identification of a range of anionic dye molecules.[50] The applied matrix 9-aminoacridin (9AA) appears to be a good choice for such analytes; it allows for measurements in negative ion mode and only exhibits a low background. Measured species in MALDI-TOF mass spectrometry are virtually always singly charged. Multiply charged species therefore most often lose all of their counter ions but they will be compensated by protons from the MALDI plume to result in a singly charged ion (e.g. $[M-NH_4]^-$, $[M-2\ NH_4+H]^-$, $[M-3\ NH_4+2H]^-$, etc.).

Figure 6 shows the results of MALDI-TOF analysis of **oligo-CzA** sample. The measurements are reproducible but for older samples, the spectra feature peaks with lower molecular weight. The results suggests that the product consists of three molecular species. This is supported by preparative HPLC (Figure S13) where three different hues of purple are separated from the fresh dye sample. An older solution of the sample, that has been stored for a few weeks, gives a wider palette of colours and at least six different fractions are identified.

Taking the results from MALDI-TOF and the structural analysis into consideration, we can make a few suggestions on the molecular structure. For examples the major peak at 548.16 m/z in the fresh sample corresponds closely the original structure suggested (Figure 7, left). However, we do not know on which position the individual CzA units are connected, so the structure might also resemble the right proposal in Figure 7. This would also account for the radical character of the product in form of a non-Kekulé structure. However, it should be

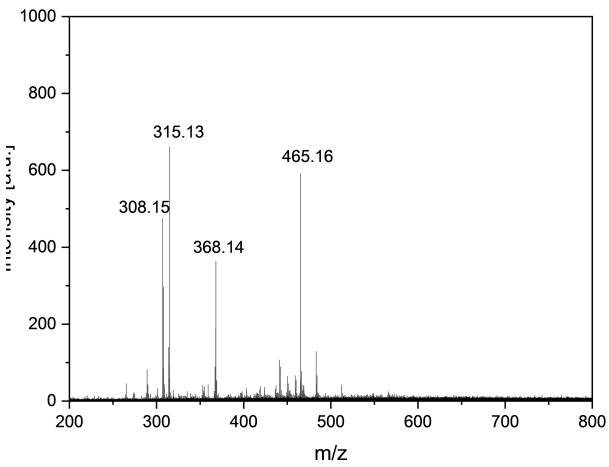

Figure 6. MALDI-TOF mass spectrometry measurements of **oligo-CzA**, freshly prepared (left) and after a few weeks, stored as powder (right). The measurement took place in negative ion mode and by using 9AA as a matrix. The laser intensity was 40%.

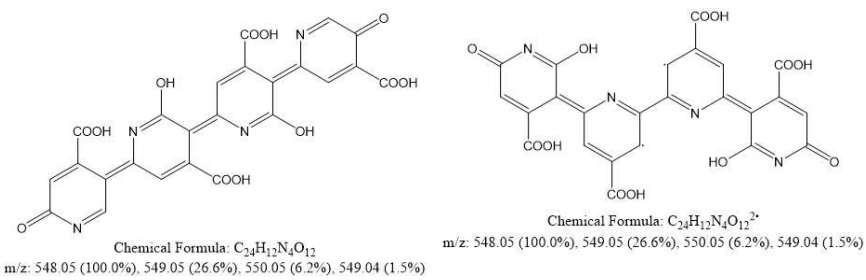

Figure 7. Proposals for the structure of the major component of **oligo-CzA**.

stressed, that more work will be required to advance on this subject and the nature of the stable free radical. For example, in the present investigation we did not resolve weather we are dealing with a monoradical or diradicals.

Spectral Properties

The purified product features high solubility in water and results in a solution with an intense purple colour, which is even stronger in ammonia solution. However, the colour of the solution fades over time – a process which is even faster in ammonia solution as well as under light illumination (Figure 8a). We presume that the highly substituted structure of **oligo-CzA** has little stability in solution due to steric hindrance within the molecules. What can also be observed in water solution, is precipitation of a purple powder. We attribute this to molecular aggregation, which is a phenomenon that is well known in dye chemistry.[51,52] This is supported by XRD measurements of the precipitate, which gives the typical signal from π-stacking at 26 °2Θ (Figure S15) as well as by the broadening of absorption band in the UV–vis spectra. Precipitation is not observed in ammonia solution. As a results, no material is retained by a dialysis tube (molecular weight cut-off 1000 Da) in case **oligo-CzA** is dissolved in ammonia solution. However, dialysis of **oligo-CzA** in water results in an initial yellow dialysate. The solution shows a single absorption peak at 340 nm which correlates to the absorption peak of CzA (Figure S16).

The fluorescent properties of the product in solution are shown in Figure 8b. There are two fluorescent centers so we assume to be dealing with two main species. The two emission maxima appear at 462 and 594 nm corresponding to excitation maxima at 370 or 558 nm, respectively. The rather large Stokes shifts of 92 and 36 nm, respectively, are related to the highly polar solvation environment (Figure S17). Notably, the fluorescence intensity decays rapidly after the product is dissolved. For example, upon continuous emission measurement at the excitation wavelength of 520 nm, a significant decay down to ~15% after 10 h is measured (Figure 8c). A decay takes place irrespective whether or not the solution was exposed to light. However, the respective emission curves differ slightly (Figure S18), which again points towards the contribution of photodegradation. The decrease of the molecular species that emits at 460 nm is less pronounced. The fluorescence quantum yields (QY_{fl}) of **oligo-CzA** were determined by the gradient method using Rhodamine B (RhB) as a reference. In ammonia in water solutions the fluorescence quantum yields are 1.9% while in ammonia in methanol the QY_{fl} is ten times higher, namely 19% (Figure S19).

Conclusions

We investigated the reaction between ammonium formate and citric acid under isochoric and solvent-free conditions. Reaction kinetics were analyzed with UV–vis spectroscopy and optimized with respect to the purple coloured reaction product. The intense purple colour of the purified reaction product indicates a yet undiscovered reaction pathway in the otherwise well studied research field of fluorophores and CNDs from citric acid. Therefore, we hypothesized that formic acid plays a pivotal catalytic role in the reaction system, which results in subsequent oligomerization of citrazinic acid derivatives. Structural similarities between the purified product and the ammonium

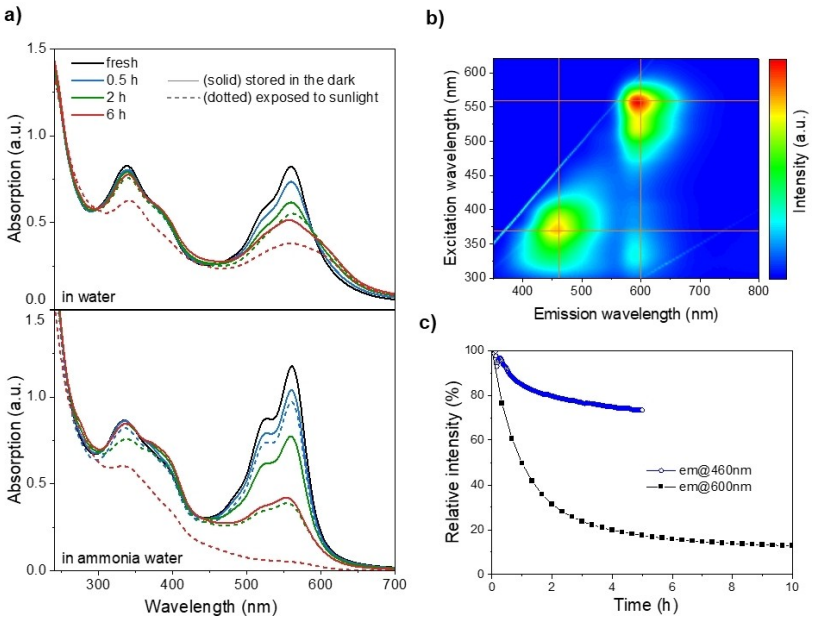

Figure 8. a) Absorption spectra of **oligo-CzA** in water as well as in ammonia water (5%). The solutions were freshly prepared (black) and then stored under dark (solid) as well as light exposed (dotted) conditions; b) 2D-photoluminescence plot of **oligo-CzA** in ammonia water; c) Fluorescence intensity decay of **oligo-CzA** in ammonia water at 460 nm (blue) and at 600 nm (black) under continuous illumination at 370 or 560 nm respectively.

salt of citrazinic acid were confirmed with several analysis techniques such as XPS, FTIR, and elemental analysis. Furthermore, EPR spectroscopy detected stable free electrons in the product structure as well as in the ammonium salt of citrazinic acid. Further analysis will be needed in order to understand these paramagnetic properties and to gain confidence with respect to the molecular structure of the product. This may also contribute to a better understanding of the formation of fluorophores and CNDs from citric acid in general.

Experimental

Synthesis in Autoclave: 3.78 g of ammonium formate was mixed with the 5.76 g of citric acid to result in a molar ratio 2:1. The mixture was thoroughly grinded in agar mortar to obtain homogeneous viscous paste. The viscous mixture was transferred into the Teflon beaker and sealed with the Teflon cap. The beaker was placed into the high-pressure stainless-steel reactor from Parr. The reactor was kept at 180 °C for 4 hours. The reaction in the reactor was stopped by cooling the autoclave in the ice bath. The product is a viscous solution with the dark colour.

Microwave Synthesis: Synthetic procedure was also performed in laboratory microwave reactor. The precursors were mixed in the same ratio (2:1 ammonium formate: citric acid), but the quantity was decreased by half to fit the pressure limit of the microwave of 18 bar. The reactants were transferred into a 35 ml quartz vial, sealed with a Teflon-lined cap. The vial was heated with a laboratory microwave (Discover SP), using a power of 50 Watt. The reaction was performed at 180 °C, but the reaction time was decreased to 40 min since stirring could be applied.

Purification Procedure: The viscous liquid product was transferred to a plastic centrifuge tube and ethanol was added. The mixture was thoroughly shacked and subsequently sonicated for 15 min in the lab sonicator. The insoluble in ethanol product was separated by centrifuging at 6000 RPM for 5 min. The washing procedure with ethanol was repeated several times, until no organic molecules were detected in the washing solution by NMR. The washed powder dried in the oven at 60 °C overnight. For 1.5 g of CA, approximately 0.7 g of purified product could be obtained (after microwave synthesis).

Preparation of NH_4-CzA: Citrazinic acid was dissolved in a minimum amount of ammonium hydroxide solution and dried in the oven at 60 °C overnight.

Analysis: *Ultraviolet-visible absorption (UV–vis)* measurements were performed with a Specord 210 plus from Analytik Jena using 10 mm quartz cuvettes. *Gel permeation chromatography (GPC)* was carried out in $H_2O/NaNO_3$ on a SUPREMA 30/3000-10 μm column. The sample was detected with a refractive index detector as well as a UV-detector at 350 nm. The molecular weight was evaluated against a poly(acrylic acid sodium salt) standard. *Scanning electron microscopy (SEM)* images were obtained on a LEO 1550-Gemini microscope. *Electron paramagnetic resonance (EPR)* spectroscopy was performed on a Bruker EMXnano benchtop X-Band EPR spectrometer, where the samples where measured in solid state in EPR tubes (ID 3 mm, OD 4 mm, length 250 mm). Samples were measured using a receiver gain of 40 dB an attenuation of 35 dB and 5 number of scans. *X-ray photoelectron spectroscopy (XPS)* was performed on a K-Alpha™+X-ray Photoelectron Spectrometer System (Thermo Scientific) with Hemispheric 180° dual-focus analyzer with 128-channel detector. X-ray monochromator is Micro-focused Al–Kα radiation. For the measurement, the prepared powder samples were loaded on carbon taps. *Fourier-transform infrared (FTIR)* measurements were performed using a Nicolet iS 5 FT-IR-spectrometer in conjunction with an iD5 ATR unit from Thermo Fisher Scientific. *Fluorescence measurements* were performed on a FP-8300 fluorescence spectrometer. *Differential scanning calorimetry (DSC)* was performed on a DSC 204 F1 Phoenix (Netzsch, Selb, Germany) using an platinum crucible at a heating rate of 10 °C min^{-1}. *Nuclear-magnetic resonance (NMR) spectroscopy* was performed on a 400 MHz Bruker Ascend 400. *Transmission electron microscopy* was performed using an EM 912 Omega from Zeiss operating at 120 kV. *CHNX analysis* was performed with a vario MICRO cube CHNOS elemental analyzer by Elementar Analysensysteme GmbH. The elements were detected with a thermal conductivity detector (TCD) for C, H, N and O. *Inductively Coupled Plasma Optical Emission spectroscopy (ICP-OES)* were performed on an Optima 8000 for quantification of sodium and potassium. *Maldi-TOF mass spectroscopy* was performed with an Autoflex speed detector from Bruker in negative mode using 9-aminoacridin (9AA) as a matrix. *X-ray diffraction (XRD)* was performed on a Bruker D8 Advance diffractometer in the Bragg–Brentano mode at the Cu Kα wavelength.

Acknowledgements

This work was financially supported by Max Planck Society. Open Access funding enabled and organized by Projekt DEAL.

Conflict of Interests

The authors declare no conflict of interest.

Data Availability Statement

The data that support the findings of this study are available from the corresponding author upon reasonable request.

Keywords: reactive eutectic media · citric acid · citrazinic acid · dyes · quantum dots

[1] X. Hu, L. Cheng, N. Wang, L. Sun, W. Wang, W. Liu, *RSC Adv.* **2014**, *4*, 18818–18826.
[2] S. Zhu, Q. Meng, L. Wang, J. Zhang, Y. Song, H. Jin, K. Zhang, H. Sun, H. Wang, B. Yang, *Angew. Chem. Int. Ed.* **2013**, *52*, 3953–3957.
[3] W. Shi, X. Li, H. Ma, *Angew. Chem. Int. Ed.* **2012**, *51*, 6432–6435.
[4] X. Zhai, P. Zhang, C. Liu, T. Bai, W. Li, L. Dai, W. Liu, *Chem. Commun.* **2012**, *48*, 7955–7957.
[5] F. Wang, Z. Xie, B. Zhang, Y. Liu, W. Yang, C. Liu, *Nanoscale* **2014**, *6*, 3818–3823.
[6] S. Qu, X. Wang, Q. Lu, X. Liu, L. Wang, *Angew. Chem. Int. Ed.* **2012**, *51*, 12215–12218.
[7] H. Bin Yang, Y. Qian Dong, X. Wang, S. Yun Khoo, B. Liu, C. Ming Li, *Sol. Energy Mater. Sol. Cells* **2013**, *117*, 214–218.
[8] H. Bin Yang, Y. Q. Dong, X. Wang, S. Y. Khoo, B. Liu, *ACS Appl. Mater. Interfaces* **2014**, *6*, 1092–1099.
[9] J. Bian, C. Huang, L. Wang, T. Hung, W. A. Daoud, R. Zhang, *ACS Appl. Mater. Interfaces* **2014**, *6*, 4883–4890.
[10] X. Lin, G. Gao, L. Zheng, Y. Chi, G. Chen, *Anal. Chem.* **2014**, *86*, 1223–1228.
[11] Y. Dong, R. Wang, W. Tian, Y. Chi, G. Chen, *RSC Adv.* **2014**, *4*, 3701–3705.
[12] Y. Dong, R. Wang, G. Li, C. Chen, Y. Chi, G. Chen, *Anal. Chem.* **2012**, *84*, 6220–6224.

[13] F. Yan, Y. Zou, M. Wang, X. Mu, N. Yang, L. Chen, *Sens. Actuators B* **2014**, *192*, 488–495.
[14] S. Zhu, Q. Meng, L. Wang, J. Zhang, Y. Song, H. Jin, K. Zhang, H. Sun, H. Wang, B. Yang, *Angew. Chem. Int. Ed.* **2013**, *52*, 3953–3957.
[15] A. Behrmann, A. W. Hofmann, *Ber. Dtsch. Chem. Ges.* **1884**, *17*, 2681–2699.
[16] W. J. Sell, T. H. Easterfield, *J. Chem. Soc. Trans.* **1893**, *63*, 1035–1051.
[17] T. H. Easterfield, W. J. Sell, *J. Chem. Soc. Trans.* **1894**, *65*, 28–31.
[18] A. E. Shadrin, *Process E-6*, Tuskadora, S.-Petersburg, **1992**.
[19] W. Kasprzyk, S. Bednarz, P. Żmudzki, M. Galica, D. Bogdał, *RSC Adv.* **2015**, *5*, 34795–34799.
[20] W. Kasprzyk, T. Świergosz, P. P. Romańczyk, J. Feldmann, J. K. Stolarczyk, *Nanoscale* **2022**, *14*, 14368–14384.
[21] A. Cadranel, J. T. Margraf, V. Strauss, T. Clark, D. M. Guldi, *Acc. Chem. Res.* **2019**, *52*, 955–963.
[22] G. Ragazzon, A. Cadranel, E. V. Ushakova, Y. Wang, D. M. Guldi, A. L. Rogach, N. A. Kotov, M. Prato, *Chem* **2021**, *7*, 606–628.
[23] C. Wang, V. Strauss, R. B. Kaner, *Trends Chem.* **2019**, *1*, 858–868.
[24] D. Shan, J.-T. Hsieh, X. Bai, J. Yang, *Adv. Healthcare Mater.* **2018**, *7*, 1800532.
[25] L. Vallan, H. Imahori, *ACS Appl. Electron. Mater.* **2022**, *4*, 4231–4257.
[26] J. Ren, L. Malfatti, P. Innocenzi, *C* **2021**, *7*, 2.
[27] M. Righetto, A. Privitera, I. Fortunati, D. Mosconi, M. Zerbetto, M. L. Curri, M. Corricelli, A. Moretto, S. Agnoli, L. Franco, R. Bozio, C. Ferrante, *J. Phys. Chem. Lett.* **2017**, *8*, 2236–2242.
[28] Y. Song, S. Zhu, S. Zhang, Y. Fu, L. Wang, X. Zhao, B. Yang, *J. Mater. Chem. C* **2015**, *3*, 5976–5984.
[29] V. Strauss, H. Wang, S. Delacroix, M. Ledendecker, P. Wessig, *Chem. Sci.* **2020**, *11*, 8256–8266.
[30] C. J. Reckmeier, J. Schneider, Y. Xiong, J. Häusler, P. Kasák, W. Schnick, A. L. Rogach, *Chem. Mater.* **2017**, *29*, 10352–10361.
[31] C. J. Reckmeier, J. Schneider, Y. Xiong, J. Häusler, P. Kasák, W. Schnick, A. L. Rogach, *Chem. Mater.* **2017**, *29*, 10352–10361.
[32] X. Miao, D. Qu, D. Yang, B. Nie, Y. Zhao, H. Fan, Z. Sun, *Adv. Mater.* **2018**, *30*, 1704740.
[33] S. Qu, D. Zhou, D. Li, W. Ji, P. Jing, D. Han, L. Liu, H. Zeng, D. Shen, *Adv. Mater.* **2016**, *28*, 3516–3521.
[34] S. Filonenko, A. Voelkel, M. Antonietti, *Green Chem.* **2019**, *21*, 5256–5266.
[35] H. Schneider, N. Merbouh, S. Keerthisinghe, S. Filonenko, *Green Chem.* **2022**, *24*, 9745–9754.
[36] W. Wang, B. Wang, H. Embrechts, C. Damm, A. Cadranel, V. Strauss, M. Distaso, V. Hinterberger, D. M. Guldi, W. Peukert, *RSC Adv.* **2017**, *7*, 24771–24780.
[37] M. B. Gawande, V. D. B. Bonifácio, R. Luque, P. S. Branco, R. S. Varma, *ChemSusChem* **2014**, *7*, 24–44.
[38] P. Mayurachayakul, N. Niamnont, K. Chaiseeda, O. Chantarasriwong, *Asian J. Org. Chem.* **2022**, *11*, e202200117.
[39] M. Bakthadoss, G. Murugan, *Eur. J. Org. Chem.* **2010**, *2010*, 5825–5830.
[40] J. C. Ensign, S. C. Rittenberg, *Arch. Mikrobiol.* **1965**, *51*, 384–392.
[41] N. Sutthiwong, M. Fouillaud, A. Valla, Y. Caro, L. Dufossé, *Food Res. Int.* **2014**, *65*, 156–162.
[42] B. Jana, Y. Reva, T. Scharl, V. Strauss, A. Cadranel, D. M. Guldi, *J. Am. Chem. Soc.* **2021**, *143*, 20122–20132.
[43] V. Strauss, A. Kahnt, E. M. Zolnhofer, K. Meyer, H. Maid, C. Placht, W. Bauer, T. J. Nacken, W. Peukert, S. H. Etschel, M. Halik, D. M. Guldi, *Adv. Funct. Mater.* **2016**, *26*, 7975–7985.
[44] A. B. Bourlinos, A. Stassinopoulos, D. Anglos, R. Zboril, M. Karakassides, E. P. Giannelis, *Small* **2008**, *4*, 455–458.
[45] B. Tang, J. Zhao, J.-F. Xu, X. Zhang, *Chem. Sci.* **2020**, *11*, 1192–1204.
[46] P. Murto, H. Bronstein, *J. Mater. Chem. C* **2022**, *10*, 7368–7403.
[47] Q. Song, F. Li, Z. Wang, X. Zhang, *Chem. Sci.* **2015**, *6*, 3342–3346.
[48] L. Jinshi, S. Pingchuan, Z. Zujin, T. Ben Zhong, *CCS Chem.* **2019**, *1*, 181–196.
[49] F. Sánchez-Viesca, R. Gómez, *World J. Org. Chem.* **2020**, *8*, 5–6.
[50] L. J. Soltzberg, A. Hagar, S. Kridaratikorn, A. Mattson, R. Newman, *J. Am. Soc. Mass Spectrom.* **2007**, *18*, 2001–2006.
[51] D. G. Duff, D. J. Kirkwood, D. M. Stevenson, *J. Soc. Dyers Colour.* **1977**, *93*, 303–306.
[52] D. F. Bradley, M. K. Wolf, *Proc. Nat. Acad. Sci.* **1959**, *45*, 944–952.

Manuscript received: March 13, 2023
Revised manuscript received: June 20, 2023
Accepted manuscript online: June 26, 2023
Version of record online: July 14, 2023